Journal of Power Sources 196 (2011) 7841–7846

Contents lists available at ScienceDirect

Journal of Power Sources

journal homepage: www.elsevier.com/locate/jpowsour

Facile preparation and electrochemical characterization of cobalt oxide/multi-walled carbon nanotube composites for supercapacitors

Junwei Lang, Xingbin Yan*, Qunji Xue

State Key Laboratory of Solid Lubrication, Lanzhou Institute of Chemical Physics, Chinese Academy of Sciences, Lanzhou 730000, PR China

ARTICLE INFO

Article history:
Received 28 January 2011
Received in revised form 3 April 2011
Accepted 4 April 2011
Available online 8 April 2011

Keywords:
Carbon nanotube
Cobalt oxide
Composite
Supercapacitor

ABSTRACT

A series of cobalt oxide/multi-walled carbon nanotube (Co_3O_4/MWCNT) composites are successfully synthesized by a facile chemical co-precipitation method followed by a simple thermal treatment process. The morphology and structure of as-obtained composites are characterized by X-ray diffraction, scanning electron microscopy, and N_2-adsorption/desorption measurements, and the electrochemical properties are investigated by cyclic voltammetry (CV), galvanostatic charge/discharge and electrochemical impedance spectroscopy (EIS). For all Co_3O_4/MWCNT composites, MWCNTs are well dispersed in the loosely packed Co_3O_4 nanoparticles. Among them, the Co_3O_4-5%MWCNT composite exhibits the highest specific surface area of 137 $m^2\,g^{-1}$ and a mesoporous structure with a narrow distribution of pore size from 2 to 10 nm. Because of the synergistic effects coming from Co_3O_4 nanoparticles and MWCNTs, the electrochemical performances of pure Co_3O_4 material are significantly improved after adding MWCNTs. The Co_3O_4-5%MWCNT composite shows the largest specific capacitance of 418 $F\,g^{-1}$ at a current density of 0.625 $A\,g^{-1}$ in 2 M KOH electrolyte. Furthermore, this composite exhibits good cycling stability and lifetime. Therefore, based on the above investigation, such Co_3O_4/MWCNT composite could be a potential candidate for supercapacitors.

1. Introduction

In response to the fossil fuel energy depletion and global warming issues, energy storage becomes a great challenge to the major world powers and scientific community [1,2]. With the urgent need for hybrid electric vehicle-based green transportation, high power and high energy storage devices have received much attention. In this regard, supercapacitor that possesses a higher power density than batteries and a higher energy density than conventional capacitors is probably one of the most efficient energy storage devices [3–5].

Recently, considerable attention has been paid to develop two different types of supercapacitors, including electrochemical double-layer capacitors (EDLCs), based on carbon materials with a high surface area and faradaic pseudocapacitors based on metal oxides or conducting polymers with several oxidations [6,7]. For the electrodes with the same active area, the faradic pseudocapacitors have higher energy density while the electric double-layer capacitors have higher power density. Because the performance of the supercapacitor devices strongly depends on the physicochemical properties of the electrode materials, an active electrode material with high specific capacitance and excellent rate capability is indispensable for the development of supercapacitors with both high power density and high energy density [8,9].

Cobalt oxides as typical transition metal oxides, with the consideration of low cost, natural abundance and environment safety, have been reported to be promising electrode materials for pseudocapacitors [10–12]. Cobalt oxides can interact with ions not only at the surface, but also throughout the bulk as well [2]. However, when a thick-and-compact cobalt oxide film is used for electrode fabrication, the charge-transfer-reaction kinetics is limited tremendously due to its poor electronic conductivity and difficulty in the penetration of electrolyte into it [13]. It would result in a relatively low specific capacitance and an ineffective utilization for cobalt oxide supercapacitors. Therefore, for a cobalt oxide electrode, the key strategy is to enhance its conductivity and increase its specific surface area, so that both the energy density and power density could be both improved remarkably [14].

On the other hand, among various carbonaceous electrode materials, such as mesoporous carbon [15], activated carbon [16], carbon fibers [17], carbon nanotube (CNT) [18,19] and newly developed graphene [20–22], CNT has won the privileged part of research and development as the electrode material for EDLC. It is owing to its unique one-dimensional mesoporous structure, highly accessible surface area, good electrical conductivity and high chemical stability [23]. However, the drawback of relatively low energy

* Corresponding author. Tel.: +86 931 4968055; fax: +86 931 4968055.
E-mail address: xbyan@licp.cas.cn (X. Yan).

0378-7753/$ – see front matter © 2011 Elsevier B.V. All rights reserved.
doi:10.1016/j.jpowsour.2011.04.010

density restricts the development of CNT-based EDLCs. Therefore, much effort has been paid to use CNTs as additives and/or the substrates for depositing active metal oxides in order to develop metal oxide/CNT composite supercapacitors with high power density and high energy density [24–26].

Therefore, cobalt oxide/CNT composites with highly conductive CNT compound and highly pseudocapacitive cobalt oxide compound, are of great interest when each constituent component provides specific functions for high performance applications. However, to date few reports cover the cobalt oxides-CNT composites for supercapacitor. Shan et al. synthesized MWCNTs/Co_3O_4 composite as the electrode material for supercapacitor and the specific capacitance reached up to 201 F g^{-1} [27]. The dissatisfactory capacitance limits its practical application in supercapacitors as well. These have motivated us to explore the fabrication of cobalt oxide/CNT composites with further improved capacitive performance and to study the electrochemical mechanism.

In this paper, a series of Co_3O_4/MWCNT composites were synthesized by a facile chemical co-precipitation method followed by a simple thermal treatment process. The physical and electrochemical characteristics of as-prepared composites were investigated. The results show that the electrochemical properties of pure Co_3O_4 material were significantly improved after adding MWCNTs due to the synergistic effects coming from Co_3O_4 nanoparticles and MWCNTs. The maximum specific capacitance of 418 F g^{-1} was obtained for the Co_3O_4-5%MWCNT composite in 2 M KOH electrolyte and this composite exhibited good cycling stability after running 2000 cycles.

2. Experimental

2.1. Synthesis of Co_3O_4/MWCNT composites

MWCNTs (purity, 95>%; diameter, 10–20 nm; specific surface area, 200 m^2 g^{-1}) were purchased from Chengdu Organic Chemicas Co., Ltd., China. All of the other chemicals were of analytical grade and used without further purification. A typical experimental procedure was described as followed. Firstly, MWCNTs were acid-treated with concentrated nitric acid at 140 °C for 15 h according to the procedure described in the literature [28]. Then the treated MWCNTs were rinsed with distilled water and dried at 60 °C for 24 h. Secondly, 20 mg of MWCNTs was subsequently dispersed into each 50 ml of $CoCl_2{\cdot}6H_2O$ aqueous solution with different molar concentrations (0.14, 0.082, 0.057 and 0.024 M) by stirring and ultrasonic treatment. The pH value of each mixed solution was adjusted to 9 by adding 5 wt.% $NH_3{\cdot}H_2O$ drop-by-drop at room temperature. The resulting suspensions were kept stirring at this temperature for 3 h. After that, the as-obtained solids were filtered, washed with distilled water several times and dried in air at 80 °C. Finally, the dried solids were placed in a muffle furnace and calcined at 250 °C in air for 6 h with a heating rate of 2 °C min^{-1}, to obtain a series of Co_3O_4/MWCNT composites with different contents of MWCNTs. The samples were denoted as Co_3O_4-*x*%MWCNT (*x* is the weight percent of MWCNTs).

2.2. Structural characterization

The morphology and microstructure of the obtained products investigated using a field emission scanning electron microscope (FESEM, JSM-6701F). Crystallite structures were determined by a XRD (X' Pert Pro, Philips) using Cu Kα radiation from 5° to 80° angles. Nitrogen adsorption–desorption isotherm measurements were performed on a Micrometitics ASAP 2020 volumetric adsorption analyzer at 77 K. The Brunauer–Emmett–Teller (BET) method was utilized to calculate the specific surface area of each sample and the pore-size distribution was derived from the adsorption branch of the corresponding isotherm using the Barrett–Joyner–Halenda (BJH) method. The total pore volume was estimated from the amount adsorbed at a relative pressure of $P/P_0 = 0.99$.

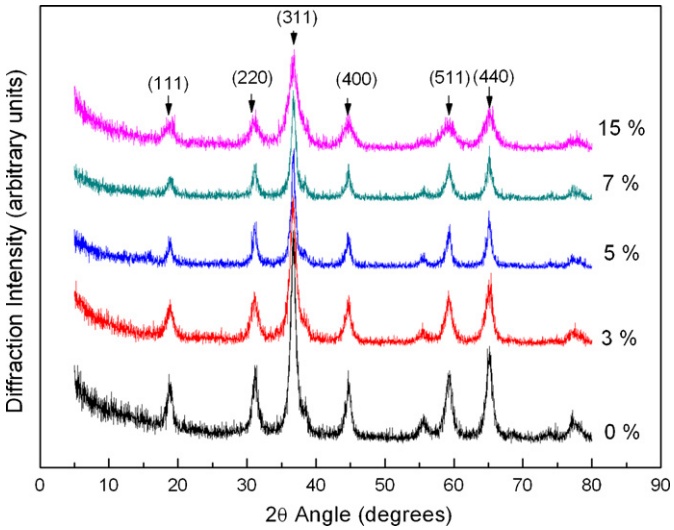

Fig. 1. The XRD patterns of the Co_3O_4/MWCNT composites with different MWCNT contents.

2.3. Electrode preparation and electrochemical measurements

The working electrodes were prepared according to the method reported in the literature [29]. 80 wt.% of Co_3O_4/MWCNT powder was mixed with 7.5 wt.% of acetylene black (>99.9%) and 7.5 wt.% of conducting graphite in an agate mortar until a homogeneous black powder was obtained. To this mixture, 5 wt.% of poly(tetrafluoroethylene) was added with a few drops of ethanol. After briefly allowing the solvent to evaporate, the resulting paste was pressed at 10 MPa to nickel gauze with a nickel wire for an electric connection. The electrode assembly was dried for 16 h at 80 °C in air. Each Co_3O_4/MWCNT electrode contained about 8 mg of electroactive material and had a geometric surface area of about 1 cm^2.

The electrochemical measurements of each as-prepared electrode were carried out using an electrochemical working station (CHI660D, Shanghai, China) in a half-cell setup configuration at room temperature. A platinum gauze electrode and a saturated calomel electrode served as the counter electrode and the reference electrode, respectively. The corresponding specific capacitance was calculated from:

$$C = \frac{I}{[(dE/dt) \times m]} \approx \frac{I}{[(\Delta E/\Delta t) \times m]} \quad (\mathrm{F\,g^{-1}}) \qquad (1)$$

where I is the constant discharging current, dE/dt indicates the slope of the discharge plot of the discharging curves, and m is the mass of the corresponding electrode material.

3. Results and discussion

3.1. Microstructure characterizations

The XRD patterns of the Co_3O_4/MWCNT composites with different MWCNT contents are shown in Fig. 1. For the pure Co_3O_4 sample, all diffraction peaks were perfectly indexed into the spinel Co_3O_4 crystal (PDF, card no. 42-1467). In comparison, for all Co_3O_4/MWCNT composites, all diffraction peaks were still in good accordance with the spinel Co_3O_4 structure and no obvious peak

of MWCNTs was observed in each pattern. Moreover, with increasing MWCNT content, the intensity of all diffraction peaks decreased gradually, indicating the loosely packed coating of Co_3O_4 on MWCNTs [27]. This is due to that the MWCNTs with entangled network and high specific surface area acted as a loose 3-dimensional template for growing Co_3O_4 crystallites, as a result of the loose packing of Co_3O_4 on MWCNTs.

To further investigate the surface morphology of as-prepared Co_3O_4/MWCNT composites, SEM measurement was employed. Fig. 2a and b shows the SEM images of pure Co_3O_4 powder and Co_3O_4-5%MWCNT composite, respectively. It can be seen that pure Co_3O_4 product was composed of nanoparticles with the sizes of dozens of nanometers. The composite product showed the similar grain-like morphology except that scattered MWCNTs coated with nanoparticles were observable. It indicated that the MWCNTs were well-dispersed into Co_3O_4 matrix. Because the electrical conductivity of the Co_3O_4 is very low, the well-dispersed MWCNTs in the Co_3O_4 matrix would form a three-dimensional network for electronic transmission, which would improve the connectivity of Co_3O_4 particles and the electrical conductivity of the composite.

The specific surface area and pore-size distribution analyses of the Co_3O_4-MWCNT composites were conducted using N_2 adsorption and desorption experiments. Fig. 3a and b shows the N_2 adsorption–desorption isotherms of pure Co_3O_4 and Co_3O_4-5%MWCNT composite, respectively. The corresponding BJH pore-size distributions are shown in the insets. As seen from Fig. 3, the existence of the hysteresis loops in both isotherms indicated the adsorption–desorption characteristic of the porous materials, especially for the Co_3O_4-5%MWCNT sample. Moreover, pure Co_3O_4 exhibited a wide mesoporous distribution ranging from 2 nm to 40 nm while the Co_3O_4-5%MWCNT composite exhibited a narrow mesoporous distribution ranging from 2 nm to 10 nm. Table 1 summarizes the textural properties of the samples. It is obvious that pure Co_3O_4 showed a specific surface area of 82 $m^2\ g^{-1}$ and an average pore size of 13.8 nm. In comparison, after adding MWCNTs, the specific surface areas of the composites increased while the average pore sizes decreased. Among them, the Co_3O_4-5%MWCNT composite exhibited the highest specific surface area of 137 $m^2\ g^{-1}$ and the lowest average pore size of 6.2 nm.

3.2. Electrochemical test

CV and chronopotentiometry measurements were employed to evaluate the electrochemical properties and to calculate the specific capacitances of as-prepared Co_3O_4/MWCNTs composites. Fig. 4a shows the CV curves of pure MWCNT electrode at different scan rate between −1 and 0 V (vs. SCE) in 2 M KOH aqueous electrolyte. It can be seen that the MWCNT electrode deviated from idealized double-layer behaviors with a pair of broad, superimposed and reversible faradaic surface redox reactions, behaving as pseudocapacitance. It was attributed to redox reactions of the functional groups on MWCNTs. Moreover, no obvious distortion in the CV curves was observed as the sweep rate increased, suggesting a highly reversible system. These excellent CV shapes revealed a very rapid current response on voltage reversal at each end potential [8]. Fig. 4b shows CV curves of the Co_3O_4/MWCNT composites with different MWCNT content at a scan rate of 10 mV s^{-1} between −0.2 and 0.5 V (vs. SCE) in 2 M KOH aqueous electrolyte. The voltammetric current responses for all Co_3O_4/MWCNT electrodes were similar to that of pure Co_3O_4 electrode. The shapes of the CV curves indicated that their capacitance characteristic was well distinguished from that of the electric double-layer capacitance. Two quasi-reversible redox reactions

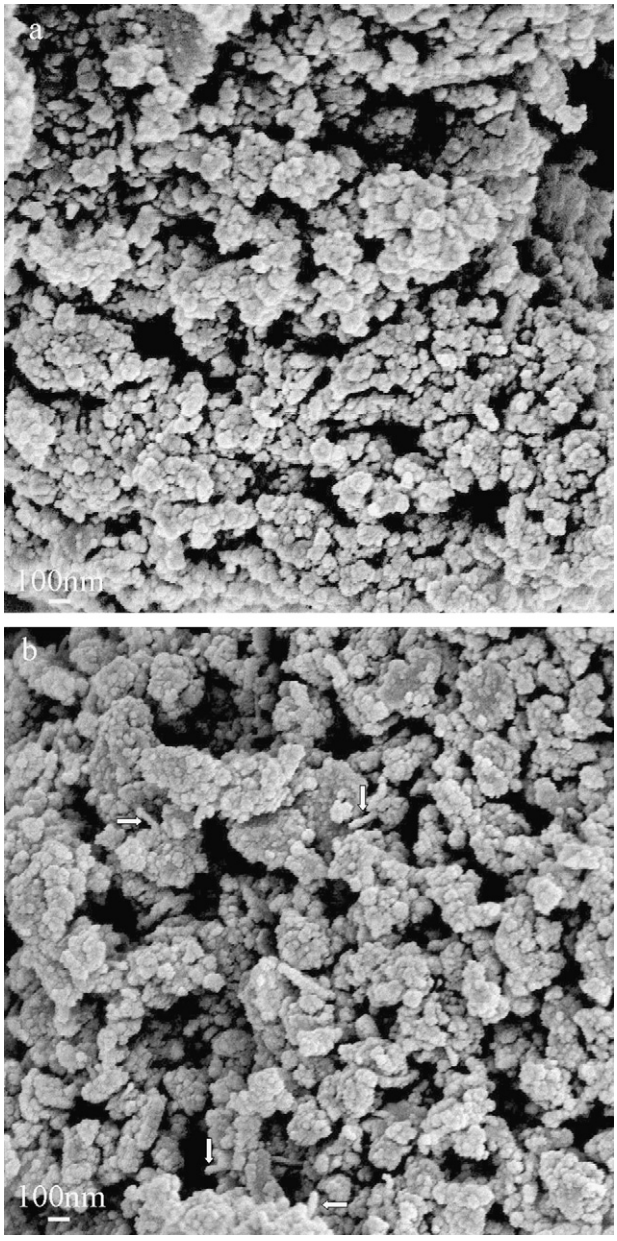

Fig. 2. SEM images of (a) pure Co_3O_4 and (b) Co_3O_4-5%MWCNT composite. Arrows show MWCNTs.

Table 1
Specific surface area, pore volume, pore size and specific capacitance of the Co_3O_4/MWCNT composites.

Weight percent of MWCNTs (wt.%)	BET specific surface area ($m^2\ g^{-1}$)	BJH pore volume ($cm^3\ g^{-1}$)	BJH pore size (nm)	Specific capacitance ($F\ g^{-1}$)
0	82	0.35	13.8	263
3	86	0.35	12.9	287
5	137	0.29	6.2	418
7	110	0.41	11.9	315
15	116	0.43	11.5	285

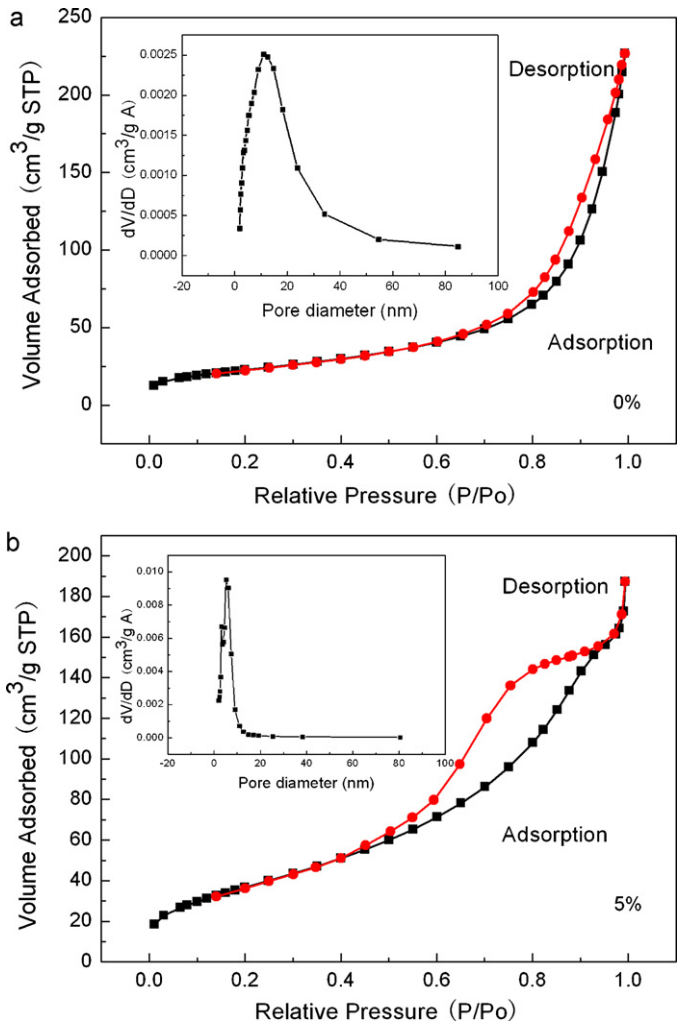

Fig. 3. N_2 adsorption–desorption isotherms of (a) pure Co_3O_4 and (b) Co_3O_4-5%MWCNT composite. The inset is the BJH pore-size distribution of the corresponding material.

occurred during the potential sweep on the Co_3O_4/MWCNT electrode [10]:

$$Co(II)_s + OH^- \leftrightarrow Co(II)(OH)_{ad} + e^- \quad Co(II)(OH)_{ad} \leftrightarrow Co(III)(OH)_{ad} + e^- \tag{2}$$

$$Co(III)_s + OH^- \leftrightarrow Co(III)(OH)_{ad} + e^- \quad Co(III)(OH)_{ad} \leftrightarrow Co(IV)(OH)_{ad} + e^- \tag{3}$$

Obviously, electrochemical polarization did not appear in all the CV curves at the two edges of potential window, indicating that a wide potential window can be chosen for the Co_3O_4/MWCNT electrodes in our system. Moreover, it is distinct that, in Fig. 4b, the Co_3O_4-5%MWCNT composite showed the largest CV area among the composites, indicating the highest specific capacitance. This is probably due to that the well dispersed MWCNTs in the Co_3O_4 provide a three-dimensional network for electronic transmission, which would improve the connectivity of Co_3O_4 particles, the electrical conductivity of the composite, and the electrochemical utilization of the pristine Co_3O_4 during the charge/discharge process. Fig. 4c shows the CV curves of the Co_3O_4-5%MWCNT electrode at different scan rates. With the increase of the sweep rate, anodic peak potential and cathodic peak potential shifted to the more anodic and more cathodic direction, respectively.

Fig. 5a shows the charge/discharge curve of pure MWCNTs electrode within a potential window of −1 to 0 V at a current density of 0.625 A g^{-1}. It is clear seen that the shape of the charge–discharge curve was closely linear and showed a typical triangle symmetrical distribution, indicating a good double layer

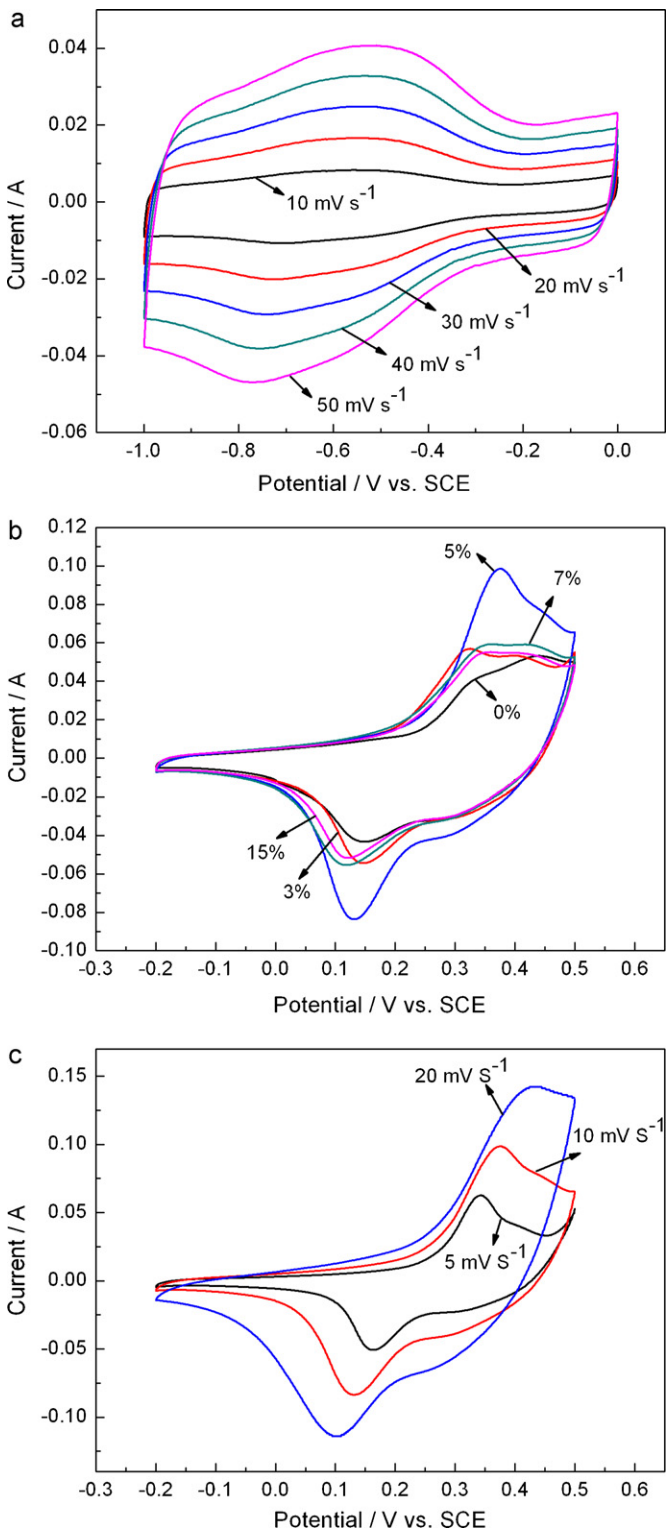

Fig. 4. CV curves of (a) pure MWCNT electrode at different sweep rate, (b) Co_3O_4/MWCNT electrodes with different MWCNT contents at sweep rate of 10 mV s^{-1} and (c) Co_3O_4-5%MWCNT electrode at different scan rates.

capacitive property. Fig. 5b shows the charge–discharge curves of the Co_3O_4/MWCNT composites with different MWCNT content in the potential range of −0.2 to 0.4 V in 2 M KOH at a current density of 0.625 A g^{-1}. The shape of the charge–discharge curves did not show the characteristic of pure double-layer capacitor, rather pseudo-capacitance. It was in agreement with the result derived

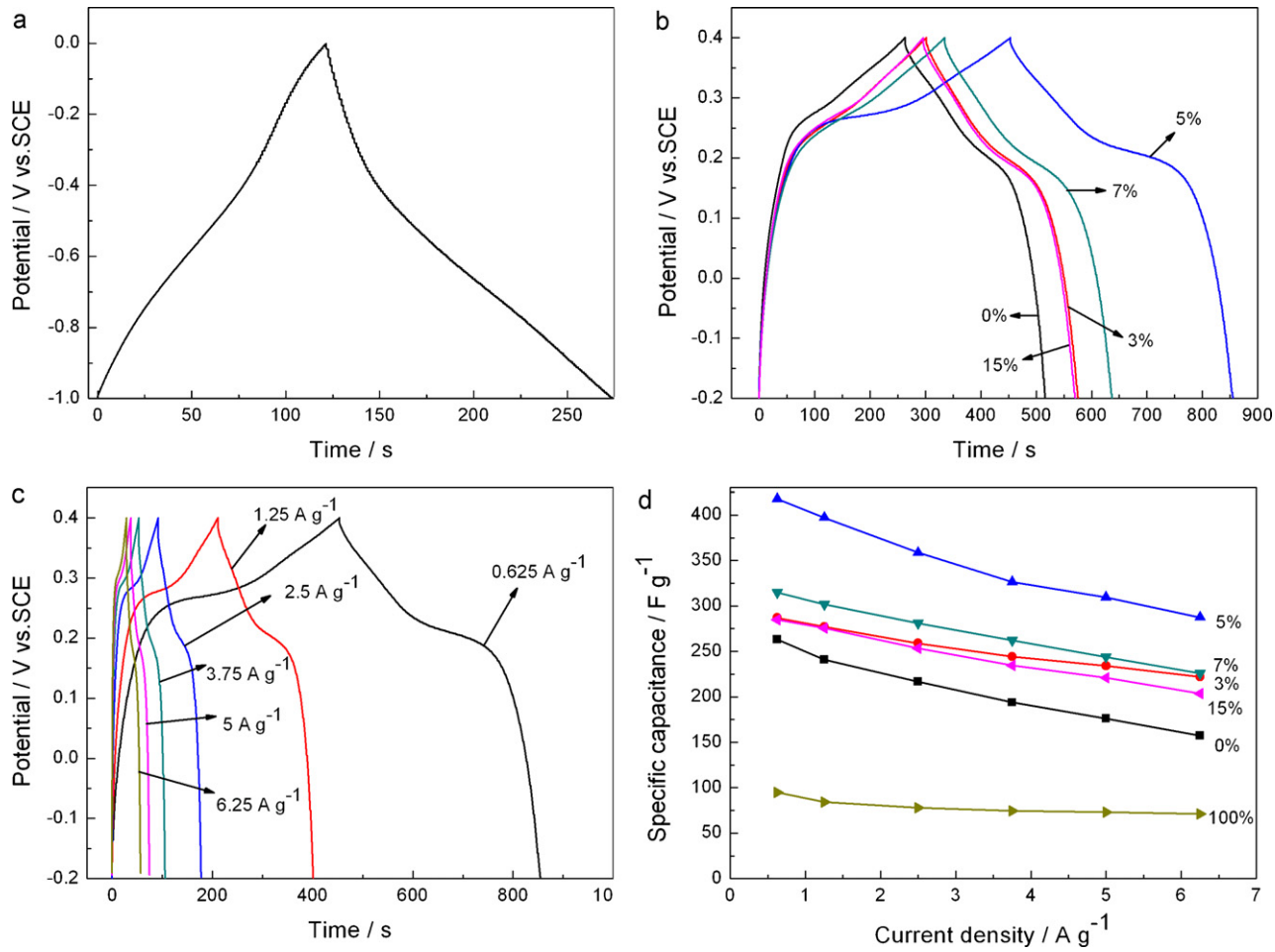

Fig. 5. (a) The charge–discharge curves of (a) pure MWCNT electrode at a current density of 0.625 A g^{-1}, (b) Co_3O_4/MWCNT electrodes with different MWCNT contents at a current density of 0.625 A g^{-1} and (c) Co_3O_4-5%MWCNT electrode at different current density. (d) The specific capacitance of the Co_3O_4/MWCNT electrodes with different MWCNT contents as a function of discharging current density.

from the CV curves. The value of the specific capacitance for pure MWCNT and Co_3O_4, Co_3O_4-3%MWCNT, Co_3O_4-5%MWCNT, Co_3O_4-7%MWCNT and Co_3O_4-15%MWCNT electrodes was calculated to be 95, 263, 287, 418, 315 and 285 F g^{-1}, respectively. It is obvious that the specific capacitance of pure Co_3O_4 electrode was significantly improved by adding MWCNTs, especially for the content of MWCNT to be 5 wt.%. Since the size range of the hydrated ions in the electrolyte is typically 6–7.6 Å and the pore size at the range of 8–50 Å is the effective one required to increase either the pseudocapacitance or electric double-layer capacitance [30]. We believed that the high specific surface area and the suitable pore size distribution of the Co_3O_4-5%MWCNT electrode were in favor of the absorption and the transport of electrolyte ions through the porous channels within the Co_3O_4-MWCNT composite. Therefore, the highest specific capacitance for the Co_3O_4-5%MWCNT electrode was mainly attributed to the effective pore size distribution and high specific surface area.

To further understand the high rate capability of the Co_3O_4/MWCNT composites, the charge/discharge measurements at different current densities were recorded. Fig. 5c displays the charge–discharge curves of the Co_3O_4-5%MWCNT composite on the current density in the range of 0.625–6.25 A g^{-1}. It is clearly seen that the specific capacitance gradually decreased with the increase of the current density. Fig. 5d further reveals that the value of the specific capacitance for each Co_3O_4-MWCNT composite was strongly dependent on the current density. In other words, the specific capacitance was inversely proportional to the current density. Moreover, under a relatively large current density of 6.25 A g^{-1}, nearly 59%, 70% and 75% of the initial value was remained for pure Co_3O_4, Co_3O_4-5%MWCNT and pure MWCNT electrode, respectively. It indicates that the Co_3O_4-5%MWCNT electrode allowed rapid ion diffusion and exhibited good electrochemical utilization. Here, MWCNTs, as a three-dimensional conducting network, facilitated OH^- soaking into Co_3O_4 particles and improved the rate capability of the Co_3O_4 particles.

EIS measurements were performed on the pure Co_3O_4 and Co_3O_4-5%MWCNT electrode, and the complex plane plots of the AC impedance spectra are shown in Fig. 6. It is seen that both impedance spectra were almost similar, composed of one semicircle component at high-frequency and followed by a linear component at the low-frequency. Moreover, a distinct knee in the frequency was observed in each curve. It should be mentioned that there were two obvious differences existing between the two spectra. One difference is the internal resistance (R_b), which includes the total resistances of the ionic resistance of electrolyte, intrinsic resistance of active materials and contact resistance at the active material/current collector interface. The R_b of pure Co_3O_4 and Co_3O_4-5%MWCNTs electrodes was 0.87 and 0.71 Ω, respectively. Another difference is that the semicircle, which associates with the surface properties of porous electrode, corresponds to the pseudo charge transfer resistance (R_{ct}). The R_{ct} of the Co_3O_4-5%MWCNT electrode was much smaller than that of the pure Co_3O_4 electrode. At the lower frequencies, a straight sloping line represents the diffusive resistance (warburg impedance) of the electrolyte in electrode

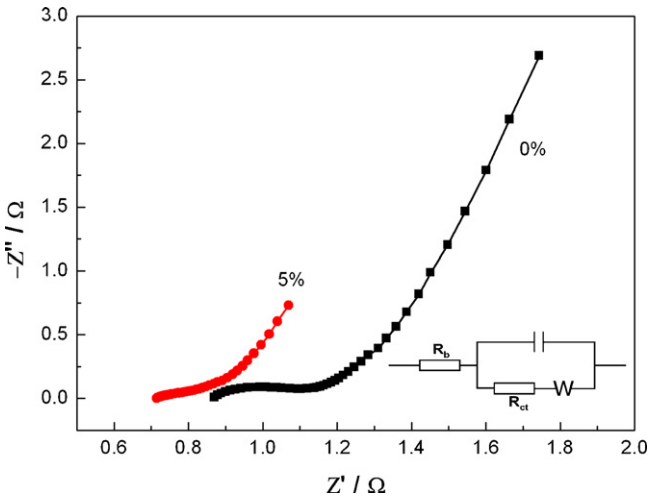

Fig. 6. Complex-plane impedance plots of pure Co_3O_4 and Co_3O_4-5%MWCNT electrode. The inset is the equivalent circuit.

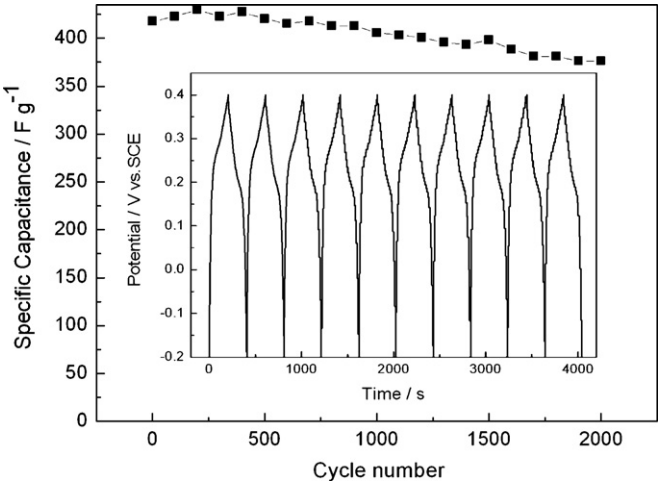

Fig. 7. Cycle life of the Co_3O_4-5%MWCNT electrode at the current densities of 1.25 A g^{-1}. The inset is first ten charge/discharge curves of the Co_3O_4-5%MWCNT electrode.

pores and the proton diffusion in host materials. Both the spectra showed higher angles than 45°, indicating the suitability of the Co_3O_4-based materials as the electrode materials for supercapacitors [31,32]. Therefore, the EIS data showed that the electrical conductivity of the Co_3O_4 electrode was greatly improved by the presence of MWCNTs.

The cycle life of the Co_3O_4-5%MWCNT electrode was monitored by a chronopotentiometry measurement at 1.25 A g^{-1} in 2 M KOH. As shown in Fig. 7, the specific capacitance of the Co_3O_4-5%MWCNT electrode decreased gradually with the increase of the cycle number. After a continuous 2000 cycling, the value of the specific capacitance remained 91% of the initial value. The demonstrates that, within the voltage window −0.2 to 0.4 V, the repeating charge and discharge behavior did not seem to induce significant structural or micro-structural change of the Co_3O_4-5%MWCNT electrode. The long-term stability implies that the Co_3O_4-5%MWCNT composite is an excellent electrode material for supercapacitors.

4. Conclusions

In summary, a series of Co_3O_4/MWCNT composites were successfully synthesized by a facile chemical co-precipitation method followed by a simple thermal treatment process. The well dispersed MWCNTs acted as a loose 3-dimensional template for growing Co_3O_4 crystallites, as a result of the improvement of the connectivity between Co_3O_4 particles, the electrical conductivity of the composite and the electrochemical utilization of the pristine Co_3O_4 during the charge/discharge process. Among them, the Co_3O_4-5%MWCNT composite showed the largest specific capacitance and good cycling stability. Therefore, based on the above investigation, such Co_3O_4-5%MWCNT composite could be a promising candidate for supercapacitors.

Acknowledgements

This work was supported by the Top Hundred Talents Program of Chinese Academy of Sciences, the National Basic Research 973 Program of China, the National Nature Science Foundations of China (51005225) and the Postdoctoral Science Foundation of China (20100480728).

References

[1] M. Winter, R.J. Brodd, Chem. Rev. 104 (2004) 4245–4269.
[2] S.L. Xiong, C.Z. Yuan, X.G. Zhang, B.J. Xi, Y.T. Qian, Chem. Eur. J. 15 (2009) 5320–5326.
[3] B.E. Conway, Electrochemical Supercapacitors Scientific Fundamentals and Technological Applications, Kluwer Academic/Plenum Publishers, New York, 1999.
[4] A. Burke, J. Power sources 91 (2000) 37–50.
[5] J.W. Lang, L.B. Kong, W.J. Wu, Y.C. Luo, L. Kang, Chem. Commun. 35 (2008) 4213–4215.
[6] R. Kötz, M. Carlen, Electrochim. Acta 45 (2000) 2483–2498.
[7] J.S. Huang, B.G. Sumpter, V. Meunier, Angew. Chem. Int. Ed. 47 (2008) 520–524.
[8] J. Yan, Z.J. Fan, T. Wei, J. Cheng, B. Shao, K. Wang, L.P. Song, M.L. Zhang, J. Power sources 194 (2009) 1202–1207.
[9] H. Zhang, G.P. Cao, Y.S. Yang, Energy Environ. Sci. 2 (2009) 932–943.
[10] L.B. Kong, J.W. Lang, M. Liu, Y.C. Luo, L. Kang, J. Power sources 194 (2009) 1194–1201.
[11] Y.Y. Gao, S.L. Chen, D.X. Cao, G.L. Wang, J.L. Yin, J. Power sources 195 (2010) 1757–1760.
[12] J.K. Lee, G.P. Kim, K.H. Kim, I.K. Song, S.H. Baeck, J. Nanosci. Nanotechnol. 10 (2010) 3676–3679.
[13] S.R. Sivakkumar, J.M. Ko, D.Y. Kim, B.C. Kim, G.G. Wallace, Electrochim. Acta 52 (2007) 7377–7385.
[14] P. Lin, Q.J. She, B.L. Hong, X.J. Liu, Y.N. Shi, Z. Shi, M.S. Zheng, Q.F. Dong, J. Electrochem. Soc. 157 (2010) A818–A823.
[15] C.T. Hsieh, Y.T. Lin, Micropor. Mesopor. Mater. 93 (2006) 232–239.
[16] D.H. Jurcakova, M. Seredych, G.Q. Lu, T.J. Bandosz, Adv. Funct. Mater. 18 (2008) 1–10.
[17] X.Y. Tao, X.B. Zhang, L. Zhang, J.P. Cheng, F. Liu, J.H. Luo, Z.Q. Luo, H.J. Geise, Carbon 44 (2006) 1425–1428.
[18] K.H. An, W.S. Kim, Y.S. Park, Y.C. Choi, S.M. Lee, D.C. Chung, D.J. Bae, S.C. Lim, Y.H. Lee, Adv. Mater. 13 (2001) 497–500.
[19] W. Lu, L.T. Qu, K. Henry, L.M. Dai, J. Power Sources 189 (2009) 1270–1277.
[20] X.B. Yan, J.T. Chen, J. Yang, Q.J. Xue, P. Miele, Appl. Mater. Interfaces 2 (2010) 2521–2529.
[21] Z.S. Wu, W.C. Ren, L. Wen, L.B. Gao, J.P. Zhao, Z.P. Chen, G.M. Zhou, F. Li, H.M. Cheng, ACS Nano 4 (2010) 3187–3194.
[22] Z.S. Wu, D.W. Wang, W.C. Ren, J.P. Zhao, G.M. Zhou, F. Li, H.M. Cheng, Adv. Funct. Mater. 20 (2010) 3595–3602.
[23] Q.Y. Li, Z.S. Li, L. Lin, X.Y. Wang, Y.F. Wang, C.H. Zhang, H.Q. Wang, Chem. Eng. J. 156 (2010) 500–504.
[24] X.R. Liu, T.A. Huber, M.C. Kopac, P.G. Pickup, Electrochim. Acta 54 (2009) 7141–7147.
[25] J.M. Ko, K.M. Kim, Mater. Chem. Phys. 114 (2009) 837–841.
[26] C.Z. Yuan, S.L. Xiong, X.G. Zhang, L.F. Shen, F. Zhang, B. Gao, L.H. Su, Nano Res. 2 (2009) 722–732.
[27] Y. Shan, L. Gao, Mater. Chem. Phys. 103 (2007) 206–210.
[28] W. Chen, X.L. Pan, X.H. Bao, J. Am. Chem. Soc. 129 (2007) 7421–7426.
[29] J.W. Lang, L.B. Kong, M. Liu, Y.C. Luo, L. Kang, J. Electrochem. Soc. 157 (2010) A1341–A1346.
[30] L. Cao, M. Lu, H.L. Li, J. Electrochem. Soc. 152 (2005) A871–A875.
[31] M.W. Xu, D.D. Zhao, S.J. Bao, H.L. Li, J. Solid State Electrochem. 11 (2007) 1101–1107.
[32] S.S. Zhang, K. Xu, T.R. Jow, Electrochim. Acta 49 (2004) 1057–1061.